
TÜRKİYE CUMHURİYETİ'NİN YÜZÜNCÜ YILI
In Molecular Analysis:
The Mystery of the Realm of
Spectroscopic Techniques and
Thermodynamic Properties
Editör
Cem Cüneyt Ersanlı
BİDGE

BIDGE Publications

In Molecular Analysis: The Mystery of the Realm of Spectroscopic Techniques and Thermodynamic Properties

Editor: Prof. Dr. Cem Cüneyt Ersanlı

ISBN: 978-625-6707-51-1

Page Layout: Gözde YÜCEL
1st Edition:
Publication Date: 25.12.2023
BIDGE Publications,

Certificate No: 71374

www.bidgeyayinlari.com.tr - bidgeyayinlari@gmail.com

Krc Bilişim Ticaret ve Organizasyon Ltd. Şti.
Güzeltepe Mahallesi Abidin Daver Sokak Sefer Apartmanı No: 7/9 Çankaya / Ankara

PREFACE

Dear Readers,

We are excited to bring you this work that will take you deep into the molecular world. Science is a reflection of humanity's passion for exploring unknown frontiers. This passion is constantly fueled by the desire to acquire new knowledge and insights. This book brings together a series of important studies that aim to delve deeper into scientific knowledge. “In Molecular Analysis: The Mystery of the Realm of Spectroscopic Techniques and Thermodynamic Properties” aims to provide readers who wish to understand the subtle fabric of science with a guide to unlock the doors of the molecular world and unravel its mysteries.

The overall goal of our book is to explore molecular analysis through unique perspectives arising from the combination of spectroscopic techniques and thermodynamic properties. The combination of thermodynamic principles with the insights provided by spectroscopic techniques is the main focus of this book in order to understand and extend the understanding of the complexity of the molecular world.

This book aims to not only provide readers with a scientific perspective, but also to inspire them to push the boundaries of the molecular world by arousing their scientific curiosity. It is intended as a comprehensive resource for both students and experts to understand the fundamentals of molecular analysis and deepen their knowledge in this field. We hope that “In Molecular Analysis: The Mystery of the Realm of Spectroscopic Techniques and Thermodynamic Properties” will take you on this magical journey, bring you together with science and deepen your curiosity.

We wish you a good reading.

Editor

Prof.Dr. Cem Cüneyt ERSANLI

Sinop University, Faculty of Arts and Sciences, Department of Physics, SİNOP

Contents

CHAPTER I

Characteristic Properties of Manganese (II) Center in Micro-crystalline CaCO3 at Low Temperature: An Electron Paramagnetic Resonance Investigation

Özgül KARATAŞ[1]

Introduction

It is becoming increasingly clear that knowing possible lattice site energies and symmetries is necessary to understand how a transition metal ion distributes itself in a mineral. So much so that the substitution of the transition metal ion causes a decrease in symmetry in crystals and gives rise to some interesting spectral features. Electron Paramagnetic Resonance (EPR) is the most adequate technique to identify and characterize a great variety of paramagnetic ions, such as Mn^{2+}, Fe^{3+}, and V^{4+}, in minerals (Duliu

[1] Assist. Prof. Dr., Konya Technical University, Vocational School of Technical Sciences, Department of Electricity and Energy, Nuclear Technology and Radiation Safety Program, Orcid: 0000-0003-3848-5800

vd., 2019:2; Covaci ve Duliu 2013:2; Low ve Zeira, 1972: 1115; Pwa ve Van Moort 1999:156; Shepherd ve Graham, 1984:383; Duliu vd., 2019:2). It provides valuable information about the oxidation states of transition metal ions and their site symmetry with respect to surrounding ligands. This method used in this study is based on the relationship between paramagnetic resonance and impurity in the calcite ($CaCO_3$) mineral.

Most minerals contain a number of paramagnetic ions; such that natural calcite ($CaCO_3$) often shows traces of divalent manganese (II) (Mn^{2+}). Manganese, which is among the first category of paramagnetic centers, has been investigated by many authorities for different natural calcite materials (Garribba, ve Micera, 2006:11; El Ali vd., 1993:189; Duliu, vd., 2019:3-15; Covaci ve Duliu 2013:1). This present work was carried out with the idea of obtaining more information about the EPR spectra of Mn^{2+}in natural calcite at low temperatures.

Material and Methods

The polycrystalline sample that was used in this study was prepared by grinding a vessel fragment. Firstly, the studied sample was washed with pure water and alcohol, respectively, and then it was dried for two days at room temperature to protect it from dust. After that, it was grinded slowly and separated (< 250 μm) by sieving. Approximately 200 mg of powder sample was used for EPR and XRD measurements.

The mineralogical components of the sample were investigated using a Europe GNR 600 diffractometer equipped with a CuKα source (40 mA, 40 kV) at room temperature. Sample was analyzed from $2\theta = 2°$ to 80° with 0.02° s/step.

EPR spectra of the powdered sample were performed between 4.2 – 298 K using a Bruker model X-band spectrometer supported by a standard helium flow cryostat. The powdered sample was placed in a quartz tube with an inner diameter of 3mm, and all

spectra were recorded using the same modulation amplitude for a microwave power of 0.2 mW for comparison.

Results and Discussion

X-ray Diffraction (XRD) Analysis

The XRD spectral pattern was recorded to investigate the mineral phases in the studied sample, and it is given in Figure 1. As shown in the figure, different diffraction peaks were observed, indicating the crystallinity structure in the sample. Analysis of the pattern revealed that this sample consists predominantly of calcite, and the dominant lines (as at $2\theta \sim 29.6^{\circ}$.) belonged to this mineral. Additionally, it was determined that the minor phase in the structure was quartz.

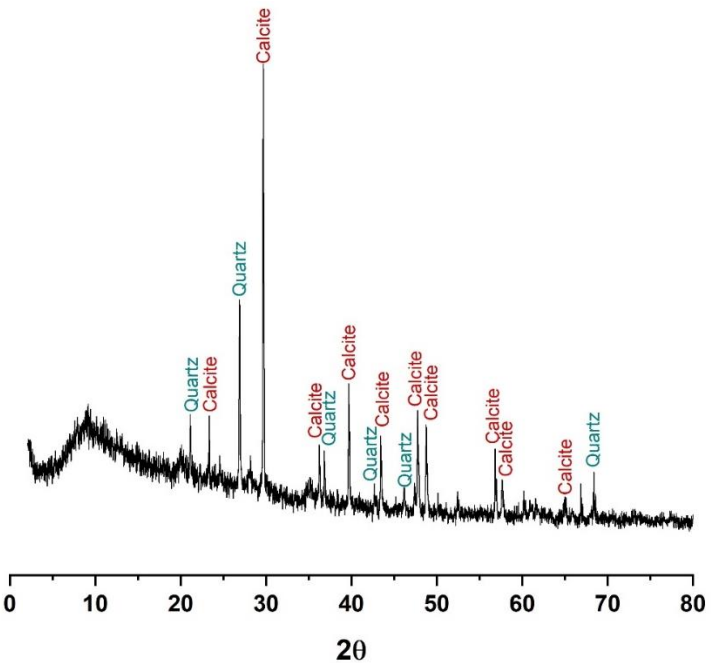

Figure 1. *XRD powder pattern showing both major (calcite) and minor (quartz) mineralogical components of the sample*

Electron Paramagnetic Resonance (EPR) Analysis

A typical EPR spectrum of the powdered sample recorded at room temperature is shown in Figure 2. It was observed that the main resonance signal contains six hyperfine lines of Mn^{2+} in accordance with the mineralogical composition. The signal intensity was correlated with the concentration of Mn^{2+} in the mineral. The hyperfine coupling constant was calculated as 9 mT and g-factor was determined around g=2 at 298K. Additionally, the presence of a free radical (g = 2.004) located between the third and fourth lines, which was thought to have formed during the firing of the sample, was observed.

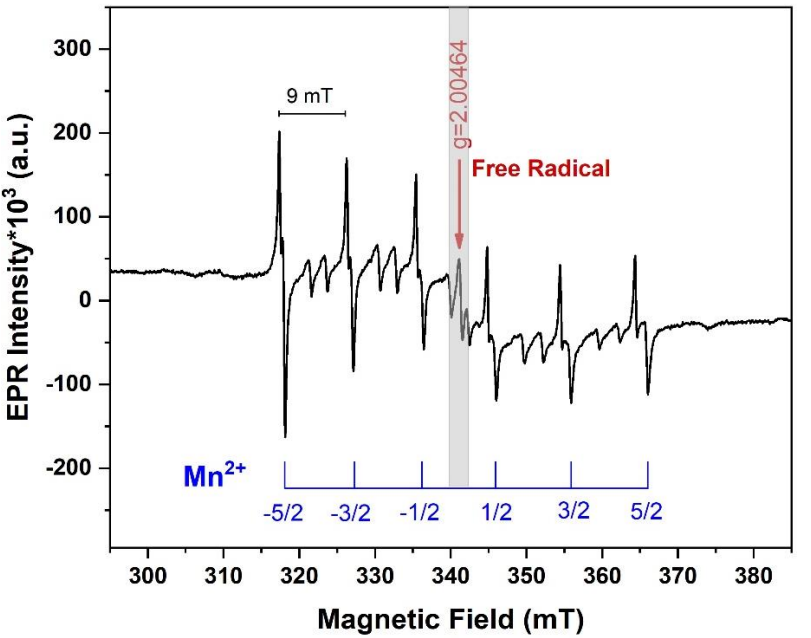

Figure 2. *The characteristic X-band EPR spectrum of Mn^{2+} ion in calcite recorded at 298 K*

Mn^{2+} spectrum consists of six lines of hyperfine structure due to the hyperfine interaction between nuclear spin I=5/2 and the effective electronic spin S=5/2 (electronic transition within the ±1/2

Kramers doublet) (Duliu, vd., 2019:6). Thus, these six hyperfine lines appeared from the allowed transitions of Mn^{2+} ions. It was understood that the calcium atoms in the calcium carbonate lattice of calcite were replaced by manganese ions (Wildeman, 1970:1967), thus forming the characteristic spectrum shown in Figure 2.

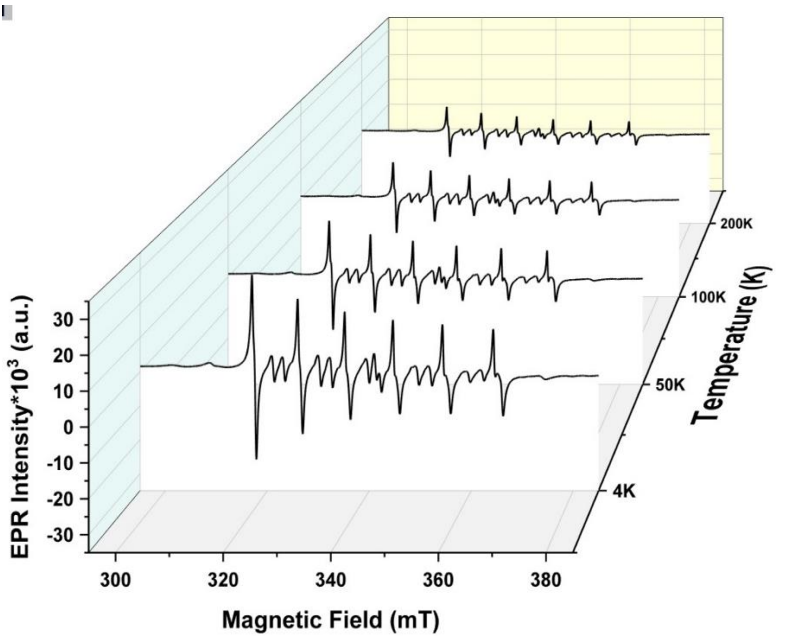

Figure 3. *X-band EPR spectra of Mn^{2+} ion in calcite recorded at different temperatures*

The effect of variable temperature on EPR signal was investigated. For this, the measuring temperature of the cavity decreased down from 298 to 4.2 K gradually. Figure 3 represents the EPR spectra of Mn^{2+} ion in calcite recorded at different temperature. It was clearly seen in the figure that, as the temperature decreased, the measured signal increased with cooling. When the calculated hyperfine coupling constant parameters for each temperature, there was small changes were observed, but g-factor did not change over the temperatures.

Conclusion

In summary, the XRD patterns revealed that the studied sample contained a highly dominant calcite mineral. The results obtained from the EPR spectra of manganese in the natural calcite mineral recorded at different temperatures showed that manganese was found as Mn^{2+} in the high ionic lattice regions and was isolated in the mineral. Furthermore, little changes were observed on the spin Hamiltonien parameters depend on the temperature. A more detailed treatment of the subjects is planned for later publication.

References

Covaci, D., & Duliu, O. G. (2013). Preliminary EPR spectra database of natural carbonate of some Romanian quarries. *Rom. Rep. Phys*, *65*(2), 487-494.

Duliu, O. G., Bercu, V., & Negut, D. C. (2019). Mn2+ EPR spectroscopy for the provenance study of natural carbonates. In *Experimental Methods in the Physical Sciences* (Vol. 50, pp. 1-19). Academic Press.

Duliu, O. G., Grecu, M. N., & Cristea, C. (2009). EPR and X-ray diffraction investigation of some Greek marbles and limestones. *Romanian Reports in Physics*, *61*(3), 487-499.

El Ali, A., Barbin, V., Calas, G., Cervelle, B., Ramseyer, K., & Bouroulec, J. (1993). Mn2+-activated luminescence in dolomite, calcite and magnesite: quantitative determination of manganese and site distribution by EPR and CL spectroscopy. *Chemical Geology*, *104*(1-4), 189-202.

Garribba, E., & Micera, G. (2006). Determination of the hyperfine coupling constant and zero-field splitting in the ESR spectrum of Mn^{2+} in calcite. *Magnetic Resonance in Chemistry*, *44*(1), 11-19.

Gunasekaran, S., & Anbalagan, G. (2008). Optical absorption and EPR studies on some natural carbonate minerals. *Spectrochimica Acta Part A: Molecular and Biomolecular Spectroscopy*, *69*(2), 383-390.

Low, W., & Zeira, S. (1972). ESR spectra of Mn^{2+} in heat-treated aragonite. *American Mineralogist: Journal of Earth and Planetary Materials*, *57*(7-8), 1115-1124.

Pwa, A., & Van Moort, J. C. (1999). Electron paramagnetic resonance (EPR) spectroscopy in massive sulphide exploration, Rosebery mine area, western Tasmania, Australia. *Journal of Geochemical Exploration*, *65*(2), 155-172.

Wildeman, T. R. (1970). The distribution of Mn2+ in some carbonates by electron paramagnetic resonance. *Chemical Geology*, *5*(3), 167-177.

CHAPTER II

Structure of Kidney Stones and Spectrometric Techniques That can be Used to Determine Constructional Differences in Kidney Stones

Sevil DURDAĞI[1]
Ali Seydi BOZKURT [2]
Ahmed ALAIKHTARLU[3]

1- INTRODUCTION

Kidney stone; it is the name given to hard mineral substances that accumulate in the kidneys. Kidney stones form if calcium oxalate or uric acid is found in higher than normal concentrations in the urine. Urinary system stone disease is a common disease that

[1] Prof. Dr. Sevil DURUDAĞI, Erzincan Binali Yıldırım University, Faculty of Science and Letters, Department of Physics, Orcıd:0000-0002-4699-2207
[2] Doç. Dr. Ali Seydi BOZKURT, Erzincan Binali Yıldırım University, Faculty of Medicine, Department of Urology, Orcıd:0000-0003-3367-8523
[3] Ahmed ALAIKHTARLU, Erzincan Binali Yıldırım University, Faculty of Science and Letters, Department of Physics, Master's Student, Orcıd:0000-0002-7028-3814

affects approximately 10-15% of the population and is three times more common in men than in women. Kidney stone disease is one of the most common diseases worldwide and affects the population at rates varying between 7-13% in North America, 5-9% in Europe and 1-5% in Asia (Sorokin et al., 2017). It is a common disease affecting approximately 10-12% of men and 5-6% of women in European countries. Nutritional habits, daily fluid intake, genetic factors, gender, geography and climate, profession and age are the factors that make a difference in urinary tract stone disease (Trinchieri et al., 2017). An increase in its prevalence was observed in the second half of the twentieth century. It is also thought that this increase in prevalence may be due to the development of possible diagnostic methods. The occurrence and type of kidney stones vary not only by gender but also by age groups. In fact, calcium oxalate dihydrate stones are a stone component that is more common in the younger age group in both genders.

Nephrolithiasis (urinary stone) has a structure that includes crystal structure components and organic matrix. Although the observed symptoms are similar, they are heterogeneous in terms of crystal structure composition and etiology of kidney stones. Structural examination of urinary stones using a single chemical method is very time-consuming and insufficient as it requires stone samples of a certain size for analysis and cannot distinguish between the two commonly found calcium stones (monohydrate/dihydrate). Furthermore, no single chemical method provides information about crystal phases and cannot detect rare drug-derived or metabolic compounds such as 2,8-dihydroxyadenine (Kourambas J, et al. 2001), xanthine, or silica.

Physical-chemical and mineralogical tools are increasingly used methods to investigate the composition of urinary stones (Shamema A.A, et al. 2015). Infrared spectroscopy examination surgically removed and spontaneously eliminated stones allows us to find out their qualitative composition. Interpreting the spectra by applying a computer program facilitates the identification of urolithiasis types. Compounds found in urinary stones may be of

organic nature (oxalic acid, uric acid, xanthine, cysteine, cholesterol) and/or inorganic nature (phosphates, carbonates).

Identification of the pathological conditions involved in stone formation should be based on a careful study of the structure, as well as on the identification of the qualitative and quantitative crystal composition of urinary stones. Information about crystal structure and composition can be found using different physical methods.

The main techniques used in the qualitative and quantitative examination of kidney stones are; X-ray diffraction, Fourier transform infrared spectrophotometry, chromatography, fluorescence, polarizing crystallography, chemical microscopy, spectroscopy and photomicroscopy techniques (Manzoor M.A.P, et al. 2019, Warty Y, et al. 2020). Schneider and his colleagues compared these techniques and showed that all of them made accurate determinations regarding stone analysis (Schneider H-J et al., 1973). The most reliable methods and recommended by the European Urology Association Guidelines are the X-ray diffraction method and Fourier Transform Infrared Spectrophotometry. Especially in recent years, IR spectroscopic analysis methods have become widespread.

2- METHOD

2.1. Epidemiology

Kidney stone disease is becoming a common disease affecting human health worldwide. As countries industrialize, kidney stone patients are encountered more frequently. Since the 1990s, people with kidney stones have been found to have increased from 5% to 10% of the population.

Although kidney stones are more common in people between the ages of 20-49, they can occur at any age. In countries/cities with more industrialization, the incidence of urinary tract stones varies between 4% and 20%. The incidence of kidney stones in the United States is 10.6% in men and 7.1% in women. It has been reported that

one in every 11 Americans may develop kidney stones at least once. Bladder stones are more common than upper urinary tract stones in developing countries; this situation has been reported in the opposite way in developed countries. Another estimate is that, with global warming, the incidence of kidney stones may increase from 40% to 56% by 2050.

Kidney stones are more common in people who are overweight and prone to diabetes. It should not be forgotten that the recurrence of kidney stones is high and 50% of recurrent patients develop a second stone within 5 years after the first stone event. It is not well known what or what accelerates the process in recurrent stone formations. Therefore, it is unpredictable in which patient will have kidney stones again. Considering the high recurrence rate, careful patient follow-up and diagnosis and treatment as early as possible are required. However, there are still unanswered questions about the etiology, structural features and symptoms of kidney stone formation.

2.2. Pathophysiology

Kidney stones form from insoluble salts in the urine, and there are two basic mechanisms in this process. In the first, formation occurs when crystals come together with a non-crystalline protein (matrix) component. Salts in the urine precipitate and crystallize, and over time these crystals come together and grow large enough to cause clinical symptoms.

In the second, a Randall plaque (always containing calcium phosphate) is typically formed as a result of the stone material precipitating on the renal papillary calcium phosphate nidus, for which calcium oxalate stones are usually responsible. We can say that most stones are composed of calcium salts such as calcium oxalate and calcium phosphate, while others are of the uric acid, cysteine and magnesium ammonium phosphate (struvite) type.

In general, pathological biomineralizations cause kidney stones, but they may be of a type such as calcium oxalate, calcium

phosphate and uric acid, or may have more complex components. Although there are different chemical stages during the formation of kidney stones, different types of stones are formed as ionic components become oversaturated in this process. That is why it is necessary to examine the physical/chemical structure of kidney stones in order to understand the pathophysiology of kidney stones correctly and to develop and plan the correct techniques for treatment in the future.

2.3. Crystal Components

There are five main types with different causes of formation. Depending on your eating habits and hereditary characteristics, the possibility of your kidney stone type changing also increases.

2.3.1. Calcium Oxalate Stones

It is the most common type (approximately 70 to 80 percent) of kidney stone and occurs when the urine includes high levels of calcium and oxalates or uric acid and low levels of citrate. Stones of this type are linked to foods rich in oxalates, which are naturally found in plants and animals. Some of these foods include beets, black tea, chocolate, nuts, potatoes and spinach. To reduce the recurrence of kidney stones, your doctor may recommend dietary changes and ask you to reduce or completely eliminate the food intake mentioned above. Your doctor may also request a higher level evaluation of your urinalysis and metabolic functions.

Calcium oxalate is in monohydrate and dihydrate forms or may be present in combination with uric acid or calcium phosphate. Calcium oxalate stones typically grow on the Randall plaque (composed of calcium phosphate) at the papillary end.

2.3.2. Calcium Phosphate Stones

Calcium phosphate stones are observed due to abnormalities in the functioning of the urinary system. Although they usually occur at the same time as calcium oxalate stones, your doctor may order a

series of blood and urine tests to accurately determine the cause of stone formation.

Calcium phosphate type stones constitute 15 percent of kidney stones, but they may also be intertwined with calcium oxalate or struvite. Calcium phosphate type stones are not found mixed with uric acid type stones, as the solubility changes as the urine pH changes. There are two types of calcium phosphate stones: apatite (sometimes reported as carbonate apatite), which is the type of crystal found in bone, or calcium hydrogen phosphate (brushite). The incidence of apatite is much higher than brushite. When the urine is examined, calcium phosphate crystals are dark and amorphous.

2.3.3. Struvite Stones

Struvite stones, which are more common in women (due to the higher risk of urinary tract infection in women), occur in the upper urinary tract as a result of infections caused by urease-producing bacteria. These stones can grow very quickly, reach large sizes, and sometimes cover the entire kidney. So much so that, if left untreated, they can cause frequent and sometimes serious urinary tract infections and, as a result, loss of kidney function.

Some other names for struvite crystals include triple phosphate and magnesium ammonium phosphate carbonate apatite. It accounts for approximately 1 percent of kidney stones. If patients who have previously been diagnosed with calcium-containing kidney stones are later infected with a urease-producing bacteria, when we look at the structure of the stone, we can see that it contains calcium oxalate or calcium phosphate in addition to struvite.

2.3.4. Uric Acid Stones

When we look at this type of stone, which is more common in men, we see that it occurs more in people who do not drink enough water or eat rich in animal protein. It has also been reported that it is

more likely to occur in patients with gout, those with a family history of this type of kidney stones, or those receiving chemotherapy.

The most common crystal form containing urate is uric acid, occurring in approximately 8 percent of stones analyzed. Uric acid stones, sometimes found in combination with calcium oxalate, contain sodium urate and ammonium urate, which are among the rare crystals containing urate.

2.3.5. Cystine Stones

Cystine stones are caused by a rare inherited genetic disorder called "cystinuria" that can cause excessive amounts of cystine to accumulate in the urine. Formed when there is too much cystine in the urine, these stones can get stuck in the kidneys, bladder, or anywhere in the urinary tract. In most people with cystinuria, the disease tends to recur. It is a condition that cannot be cured, lasts a lifetime, and is constantly monitored by doctors.

2.4. Mechanisms of Kidney Stone Formation

The mechanism of kidney stone formation is a complex biochemical process related to urinary physicochemical changes and saturation, which is still not fully understood. The sequence of events in stone formation; It consists of nucleation, growth, accumulation and crystal retention in the kidneys. As a result of saturation, dissolved substances precipitate in the urine and nucleation occurs, which subsequently forms crystal deposits. Therefore, the crystallization process depends on the thermodynamics of the solution leading to nucleation and the rates of crystal growth.

The stone formation process varies depending on the stone type and urine structure. For example, crystallization of calcium-based stones (calcium oxalate or calcium phosphate) occurs if the urine is saturated if inhibitor concentrations are low.

As the crystal grows, the crystals in the urine come together and form a small but hard mass. Stone growth occurs through the

aggregation of previously formed crystals or secondary nucleation of crystals on the matrix-covered surface. When a crystal in solution comes together to form a larger stone, it is called accumulation. Crystal deposition is considered one of the most critical steps in stone formation.

2.5. Techniques Used for Analysis of Kidney Stones

Different diseases may cause kidney stones. It is important to determine the stone structure correctly in order to determine appropriate treatment methods according to the stone type, to know its etiology, to prevent recurrences and to provide personalized treatment. Correctly performed stone analyzes are important in the initial evaluation.

With spectroscopic analysis, the qualitative compositions of surgically removed or spontaneously passing stones can be determined. We can obtain more accurate and general information about the stone composition and structure, and its etiology due to the past conditions that led to the crystallization process.

Some of the basic techniques used in the analysis of kidney stones are:

2.5.1. Wet Chemical Analysis

Although with this technique we can only detect the presence of individual ions and radicals and cannot distinguish mixtures (Kasidas et al., 2004), it is one of the most widely used methods in kidney stone analysis.

2.5.2. Thermogravimetry

Thermogravimetric analysis (TG or TGA) has been applied since the seventies (Lee et al., 2012). It works on the principle of continuously recording the weight loss in your sample. Since each substance has its own transformation properties, the starting and ending temperature of the transformation, the amount of weight

change, enthalpy, the structure of the substance and the magnitude of the weight change indicate the ratio of the elements present (Kasidas et al. 2004).

Rose and Woodfine recommended this method for its rapid analysis of kidney stones (Rose & Woodfine, 1976). D'Ascenzo et al. compared the results of differential thermal analysis (DTA) with TGA in their study (D'Ascenzo et al., 1983). They stated that this technique has great accuracy as well as speed in identifying and recording the material at a certain temperature in kidney stone analysis.

2.5.3. Polarization Microscopy

The basic working principle of polarization microscopy is the interaction of crystals in the kidney stone structure with polarized light. Therefore, the color of the light, the amount of refraction, reflection or double reflection are the parameters that determine the minerals contained in the stone (Schubert G., 2006). The stone is broken and then a drop of liquid with the appropriate refractive index is dropped onto the crystal and examined under a polarizing microscope (Douglas and Tonks, 1979).

2.5.4. Scanning Electron Microscope (SEM)

Scanning electron microscopy is one of the most sensitive techniques used to examine the morphology and texture of urinary stones, especially in recent years. Surface structural characterization of kidney stones can be performed using scanning electron microscopy at various magnifications. Even if kidney stones are very small, it is possible to perform sensitive analyzes without disturbing the structure and morphology of the components (Durdağı et al. 2023). As a result of producing very high resolution images, it provides a wide range of information on the composition of the crystal, its form, size, distribution, internal structure, location of the components, crystal transformations and the close relationship between crystals and organic components (Charafi et al., 2010).

2.5.5. Infrared Spectroscopy (IR)

This method, which was first applied by Beischer for stone analysis in 1955, has since been known as the most popular and reliable method in quantitative stone analysis (Singh, 2008). Kidney stone samples to be examined are first exposed to infrared rays to create atomic and molecular vibrations. The spectra emitted by the samples are then recorded and the spectra are analyzed to determine the elemental composition of the stone (Nguyen Quy and Daudon, 1997; Kasidas et al., 2004). One of the newest techniques developed in infrared spectroscopy is attenuated total reflection (ATR), and it has become possible to obtain more sensitive and accurate results (Schubert, 2006). One of the most important advantages of ATR is that it eliminates sample preparation steps by using KBr and allows direct analysis of kidney stones. In fact, it is extremely easy to determine the identity of calcium oxalate, which is difficult to analyze with other spectrometers, with ATR-IR spectroscopy (Bazin et al., 2012). Jubayir (Jubayir HN, 2023) emphasized the sensitivity of this technique in identifying organic and inorganic components by examining a series of kidney stones.

2.5.6. Energy Dispersive X-Ray Analysis (EDXRF)

Energy-dispersive X-ray Fluorescence (EDXRF) spectrometers are powerful analytical tools designed to determine the elemental compositions of various materials, that is, to perform qualitative and quantitative analyses. By measuring the energies and intensities of the emitted X-rays, it can be determined which elements are present in the sample and in what concentrations. One of the most important features of XRF analysis is that it enables non-destructive analysis. Traditional chemical analysis methods such as ICP often require destruction/dissolution of samples, making them unusable for subsequent testing or sewage. However, XRF spectrometers allow you to examine materials without changing their properties or causing any damage to them. SEM is applied together with energy dispersive X-ray analysis (EDX) to map samples, or in other words, to analyze the types and amounts of elements on or near

the surface of kidney stones. The interaction of the electron beam with the sample surface and penetration into the depth of the sample produces X-rays that are characteristic of elements located on and near the surface of the sample.

By examining the stones with this technique, Marickar and his colleagues examined the concentration percentages of the elements and thus learned the morphological characteristics of the crystals that make up all the stones (Marickar et al., 2009). In another study, stones were examined with EDXRF and the percentage of trace elements was determined, aiming to understand the role of these elements and their relationship with the patients' diets (Srivastava et al., 2014). Ali et al. used this technique to study the shape and spatial distribution of phases identified in kidney stones, and their results were promising and compatible with other applied techniques (Uvarov et al., 2011).

2.5.7. Laser-induced breakdown spectroscopy

The formation of high-temperature plasma with a short laser pulse is the main physical basis of LIBS technology. When a short pulsed laser beam is sent and focused on the sample surface, a small volume of the sample mass is removed by a process known as Laser Ablation, i.e. through both thermal and non-thermal mechanisms. As the laser pulse ends, the plasma will begin to cool, causing the plasma to emit light with distinct spectral peaks as the electrons of atoms and ions in excited electronic states return to their ground states. The different peaks in each analyzed sample are used to determine the chemical composition. By looking at the intensities of the LIBS peaks, the concentration of trace and major elements in the sample can be measured. With LIBS data analysis, both quantitative and material separations can be performed for a wide variety of sample matrices.

LIBS is a sensitive and fast optical technique that can also be used to perform multi-element analysis of kidney stone samples (Singh and Rai, 2011). Singh et al. (2018) used the LIBS method in

the examination of kidney stones. Again, Singh and Rai, emphasized that this optical technique is a sensitive and rapid method in the analysis of kidney stones (Singh VK and Rai AK, 2011). In another study, LIBS was used to obtain the spatial distribution of trace elements in kidney stones and was stated to be a very suitable technique to obtain information about the elements within the sample (Singh et al., 2009).

2.5.8. Laser Ablation Inductively Coupled Plasma Mass Spectrometry (LA-ICP-MS)

Laser Ablation Inductively Coupled Plasma Mass Spectrometry (LA-ICP-MS) is an analytical technique that uses direct microscale sampling for elemental and stable isotope analyzes in solid materials with high sensitivity. It uses a powerful laser beam with nanosecond pulses to remove material from the surface of the sample. With the interaction of the laser with the sample surface, heating, evaporation and ionization occur in the sample material, which is called "laser ablation". The sample is then ionized in an inductively coupled plasma, transporting the atomic species as ions, separating them, and analyzing them according to their mass-to-charge ratios over time. In such a way, major and trace element compositions can be analyzed up to detection limits of 10 parts per billion (ppb) in a sample. Many solid materials can be analyzed versatilely without requiring any special treatment for sample preparation. Even very small sample quantities (from picograms to femtograms) can be measured very precisely (one part per billion).

Bu teknikle analizler verilecek

2.5.9. Atomic absorption spectroscopy (AAS)

Atomic absorption spectroscopy, often abbreviated as AAS, analyzes the concentration of elements in a liquid sample based on the energy absorbed from specific wavelengths of light (usually 190 to 900 nm). By measuring the amount of light absorbed by free ions in the sample, the concentration of these atoms is determined. By

exposing a sample to light at a specific wavelength and then measuring how much of that light is absorbed by the sample, you determine not only the presence of an element in a sample, but also the concentration of that element. It can be used to examine both solid and liquid samples, as well as detecting approximately 70 different elements. However, if you want to work with solid samples, you should know that your experiment requires additional processing.

Although not as common as other spectrometric techniques, the structure of kidney stones has also been tried to be determined using AAS spectrometry. Joost and Tessadri determined 31 different trace elements in 24 different stones with AAS (Joost J. and Tessadri R., 1987). Trace element concentrations were also investigated in the blood, urine and hair of stone patients with significant trace element content. Taha et al. (2023) investigated the effects of Cu and Zn on the biochemical and molecular properties of CaOx stones using flame atomic absorption spectrometry (FAAS). Durak et al. (1988) determined magnesium and trace elements in 29 urinary tract stones using the atomic absorption spectrophotometric method.

2.5.10. Particle Induced Emission (PIXE)

Particle-induced X-ray emission, also known as proton-induced X-ray emission (PIXE), is an analytical technique used to determine the elemental composition of a sample by measuring X-rays emitted from a sample by high-energy ion bombardment. Due to high-energy ion bombardment with different beams on excitation, it produces X-rays with energies characteristic of the target element. He^{2+} or H^{+} charged particle beams are used in PIXE spectroscopy. With excitation, it removes an electron, and when the outer shell electrons change state to fill the inner shell gap, X-rays are emitted with certain energies. The emitted X-ray energies are independent of the excitation process but are characteristic of the elements present.

Pineda et al. used micro-PIXE technology to understand and explain trace element concentrations within stones. (Pineda-Vargas

et al., 2009). In another study, they were used to map the distribution of calcium oxalate in kidney stones. This study provided important information to reveal the mechanisms of renal calculi growth and stimulation with micro-PIXE technology.

2.5.11. X-ray computed microtomography (μCT) using synchrotron radiation (SR)

In synchrotron accelerators, electron oscillation is essential in a loop with a diameter ranging from 10 meters to 100 meters (some larger than that). While the path of the electron is controlled by the magnetic field, a wide range of electromagnetic spectrum is produced, including X-rays, infrared and ultraviolet rays. The radiation produced by this type is more intense than the radiation produced by conventional X-ray devices, being highly concentrated and monochromatic. In addition, the synthesis and high brightness properties of this technique make it a very important tool to examine the distribution maps of trace elements within kidney stones (Manzoor et al., 2019).

Stevens et al. used μCT to study the mechanism of stone formation within Randall's plaque and the role of apatite in the growth process (Stevens et al., 2015). Kaiser et al. used μCT to investigate the microstructures of minerals localized in nephrolithiasis (Kaiser et al., 2011). Manzoor et al. examined the texture and pattern of trace metal deposition as well as 3D analysis of porosity and spatial variance of kidney stones with SR-μCT (Manzoor et al.,2017).

2.5.12. X-ray Absorption Near Edge Spectroscopy (XANES)

X-ray Absorption Near Edge Spectroscopy (XANES) is an analytical method used to determine the local electronic structure of an atom during a reaction or electrochemical process. This technique is often applied to monitor changes in oxidation levels of electrochemically active elements. It is a spectroscopic analysis

sensitive to element-specific and local binding that determines the partial density of unoccupied states of a molecule.

Siritapetawee J. and Pattanasiriwisawa W. (2008) recorded XANES spectra around the K edges of sulfur, phosphorus, and calcium in unknown compounds of kidney stones. They found that the XANES results were in good agreement with diffraction chart data of the same stones obtained by the X-ray powder diffraction (XRPD) technique.

2.5.13. X-ray Powder Diffraction (XRD)

X-ray powder diffraction (XRD) is a laboratory technique used primarily for phase identification of a crystalline material, where information such as chemical composition, crystal structure, crystal orientation, crystallite size, lattice stress, preferred orientation and layer thickness can be obtained non-destructively and accurately. Powder diffraction is generally easier and more convenient than single crystal diffraction because it does not require making individual crystals. Before the sample to be analyzed, it is finely ground, homogenized and the average mass composition is determined.

Durdağı et al. (2023) determined the phase composition of urinary stones taken from patients in Erzincan and its surroundings by X-Ray Diffractometer analysis. Although Orlando et al. (2012) used X-ray powder diffraction to study the phase composition of human kidney stones in Brazil. Sofińska-Chmiel W. et al. (2023) used identification methods such as Infrared spectroscopy (FTIR), X-ray diffraction (XRD) and electron microscopy with EDX detector to investigate the morphology and chemical composition of multicomponent kidney stones.

3. CONCLUSION

Analysis of the structure and composition of urinary stones can provide valuable information about the stone formation process. Our research on kidney stones since 2020 shows that each type of urinary

stones has unique microstructures, morphologies, elemental composition and distribution. Based on our studies, we can say that the formation mechanism of different urinary stones is not the same.

Various techniques used for the analysis of kidney stones have both advantages and disadvantages compared to each other. FTIR and powder XRD techniques are extremely fast, relatively simple for sample preparation, and quite capable of identifying the major phases present in the particular analysis. However, they cannot help in determining the amorphous phase and water of hydration. The thermal technique is capable of determining water of hydration in analysis, but does not provide any information about the type of impurity phase present in the main phase of the stone (e.g. phosphate or oxalate type stones). The microscopic features of the analysis can be examined by SEM, which helps determine the arrangement of the microcrystalline phase in the stone matrix. Therefore, no single technique can provide complete information about the composition and structure of urinary stones and therefore requires another suitable technique for complementary information. However, with FTIR, clinicians can obtain enough information to treat the patient appropriately. However, accurate prediction of elemental contents is only possible with techniques such as EDAX and LIPS.

REFERENCES

Bazin D, Daudon M, Combes C, Rey C, (2012). Characterization and some physicochemical aspects of pathological microcalcifications. *Chem Rev*. *112*, 5092–5120.

Charafi S, Mbarki M, Bauza AC, Prieto RM, Oussama A, Grases F, (2010). A Comparative study of two renal stone analysis methods, *Int J Nephrol Urol*, *1*(*2*), 469 -475.

Dao NQ, Daudon M, (1997). Infrared and Raman spectra of calculi. Elsevier.

D'Ascenzo G, Curini R, De Angelis, Cardarelli E, Magrì A, Miano L, (1983). Renal calculi analysis. Application of thermal analytical techniques. *Thermochim. Acta*, *62*(*2-3*), 149-169.

Douglas DE, Tonks DB, (1979). The qualitative analysis of renal calculi with the polarising microscope, *Clinical Biochemistry*, *12*(*5*), 182-183, ISSN 0009-9120, https://doi.org/10.1016/S0009-9120(79)80086-7.

Durak I, Kilic Z, Sahin A, Akpoyraz M, (1992]. Analysis of calcium, iron, copper and zinc contents of nucleus and crust parts of urinary calculi. *Urol Res*. *20*(*1*), 23–6. https://doi.org/10.1007/BF00294330.

Durdağı SD, Al- Jalawee AHH, Yalçin P, Bozkurt AS, Salcan S, (2023). Morphological Characterization and Phase Determination of Kidney Stones Using X-Ray Diffractometer and Scanning Electron Microscopy, *Chinese Journal of Physics*, *83*, 379-388, ISSN 0577-9073, https://doi.org/10.1016/j.cjph.2022.08.025.

Joost J, Tessadri R, (1987). Trace element investigations in kidney stone patients. *Eur Urol*. *13*(*4*), 264-70. doi: 10.1159/000472792. PMID: 3653168.

Jubayir HN, (2023). Fourier dönüşümlü kızılötesi (ftır) kızılötesi spektroskopi ile böbrek taşlarının incelenmesi.

(Yayımlanmış Yüksek Lisans Tezi), Erzincan Binali Yıldırım Üniversitesi, Fen Bilimleri Enstitüsü, Fizik Anabilim Dalı.

Kaiser J, Holá M, Galiová M, Novotný K, Kanický V, Martinec P, Ščučka J, Brun F, Sodini N, & Tromba G, (2011). Investigation of the microstructure and mineralogical composition of urinary calculi fragments by synchrotron radiation X-ray microtomography: a feasibility study. *Urological Research, 39*(*4*), 259–267.

Kasidas GP, Samuell CT, Weir TB, (2004). Renal stone analysis: why and how? *Ann Clin* Biochem. 41, 91–97.

Kourambas J, Byrne RR, Preminger GM, (2001). Does a ureteral access sheath facilitate ureteroscopy? *J Urol*. *165*(*3*), 789-93. PMID: 11176469.

Lee SJ, Chung CW, (2014). Health Behaviors and Risk Factors Associated with Chronic Kidney Disease in Korean Patients with Diabetes:The Fourth Korean National Health and Nutritional Examination Survey, *Asian Nursing Research*, *8*(*1*), 8-14,ISSN 1976-1317, https://doi.org/10.1016/j.anr.2013.11.001.

Manzoor MAP, Mujeeburahiman,M, Rekha PD, (2017). Association of serum biochemical panel with mineralogical composition of kidney stone in India. *Acta Medica International*, *4*(*2*), 26.

Manzoor MAP, Agrawal AK, Singh B, Mujeeburahiman M, Rekha P-D, (2019). Morphological characteristics and microstructure of kidney stones using synchrotron radiation μCT reveal the mechanism of crystal growth and aggregation in mixed stones. *PLoS ONE 14*(*3*), 1-8. e0214003. https://doi.org/10.1371/journal.pone.0214003.

Marickar YMF, Lekshmi PR, Varma L. Koshy P, (2009). EDAX versus FTIR in mixed stones. *Urol Res*, *37*, 271–276. https://doi.org/10.1007/s00240-009-0202-8.

Orlando M, Kuplich L, De Souza D, Belich H, Depianti J, Orlando CGP, … Ortiz, R, (2008). Study of calcium oxalate monohydrate of kidney stones by X-ray diffraction. *Powder Diffraction*, *23*(*S1*), 59-S64. doi:10.1154/1.2903738.

Pineda-Vargas CA. Eisa MEM, Rodgers AL, (2009), Characterization of human kidney stones using micro-PIXE and RBS: A comparative study between two different populations, *Applied Radiation and Isotopes*, *67*(*3*), 464-469. https://doi.org/10.1016/j.apradiso.2008.06.036.

Rose GA, Woodfine C, (1976). The thermogravimetric analysis of renal stones (in clinical practice). *Br J Urol*. *48*(*6*), 403-412. doi: 10.1111/j.1464-410x.1976.tb06668.x. PMID: 1009320.

Schneider HJ, Berenyi M, Hesse A, Tscharnke J, (1973). Comparative urinary stone analyses. Quantitative chemical, x-ray diffraction, infrared spectroscopy and thermo-analtytical procedures. *Int Urol Nephrol*., *5,* 9–17.

Schubert G, (2006). Stone analysis. *Urol Res*. *34*(*2*), 146-150. doi: 10.1007/s00240-005-0028-y. Epub Feb 14. PMID: 16477427.

Shamema AA, Arul KT, Kumar RS, Kalkura SN, (2015). Physicochemical analysis of urinary stones from Dharmapuri district. *Spectrochimica Acta - Part A Molecular and Biomolecular Spectroscopy*, *5*(*134*), 442-4488. doi: 10.1016/j.saa.2014.05.088. Epub 2014 Jun 21. PMID: 25033236.

Singh I, (2008). Renal geology (quantitative renal stone analysis) by Fourier transform infrared spectroscopy. *Int Urol Nephrol*. *40,* 595–602. https://doi.org/10.1007/s11255-007-9327-2.

Singh VK, Rai AK, Rai PK, Jindal PK, (2009). Cross-sectional study of kidney stones by laser-induced breakdown spectroscopy. *Lasers Med Sci. 24*(*5*), 749-59. doi: 10.1007/s10103-008-0635-2. PMID: 19104906.

Singh VP, Singh PK, Rai Ratna and Bhatt L, (2011). Enhancing earliness and productivity in summer squash through

black polymulch in Uttarakhand hills. *Progressive Horticulture*, *43*(*1*):163-165.

Singh VK, Rai AK. (2011). Prospects for laser-induced breakdown spectroscopy for biomedical applications: a review. *Lasers Med Sci*. *26*(*5*), 673-87. doi: 10.1007/s10103-011-0921-2. PMID: 21533560.

Singh VK, Sharma J, Pathak AK, Ghany CT, Gondal MA, (2018). Laser-induced breakdown spectroscopy (LIBS): a novel technology for identifying microbes causing infectious diseases. *Biophys Rev*. *10*(*5*), 1221-1239. doi: 10.1007/s12551-018-0465-9

Siritapetawee J, Pattanasiriwisawa W, (2008). An attempt at kidney stone analysis with the application of synchrotron radiation. *J Synchrotron Radiat*. *15*(*2*), 158-61. doi: 10.1107/S0909049508002938. Epub 2008 Feb 19. PMID: 18296782.

Srivastava, A, Swain KK, Vashisht B, Aggarwal P, Mete U, Acharya R, Wagh DN, Reddy AVR, (2014). Studies of kidney stones using INAA, EDXRF and XRD techniques. *Journal of Radioanalytical and Nuclear Chemistry*, *300*(*1*), 191–194. doi =10.1007/s10967-014-2939-y.

Sofińska-Chmiel W, Goliszek M, Drewniak M, Nowicka A, Kuśmierz M, Adamczuk A, Malinowska P, Maciejewski R, Tatarczak-Michalewska M, Blicharska E, (2023). Chemical Studies of Multicomponent Kidney Stones Using the Modern Advanced Research Methods. *Molecules*. *28*(*16*):*6089*, 1-25. doi: 10.3390/molecules28166089. PMID: 37630341; PMCID: PMC10458485.

Sorokin I, Mamoulakis C, Miyazawa K, Rodgers A, Talati J, Lotan Y, (2017). Epidemiology of stone disease across the world. *World J Urol*. *35*(*9*), 1301-1320. doi: 10.1007/s00345-017-2008-6. PMID: 28213860.

Stevens DJ, McKenzie K, Cui HW, Noble JG, & Turney BW, (2015). Smartphone apps for urolithiasis. *Urolithiasis*, *43*(*1*), 13–19.

Taha SAY, Shokeir AA, Mortada WI, Awadalla A, Barakat LAA, (2023). Effect of Copper and Zinc Ions on Biochemical and Molecular Characteristics of Calcium Oxalate Renal Stones: a Controlled Clinical Study. *Biol Trace Elem Res*, https://doi.org/10.1007/s12011-023-03686-0.

Trinchieri A, Croppi E, Montanari E, (2017). Obesity and urolithiasis: evidence of regional influences. *Urolithiasis*. *45*(*3*), 271-278. doi: 10.1007/s00240-016-0908-3. PMID: 27488444.

Uvarov V, Popov I, Shapur N, Abdin T, Gofrit ON, Pode D, Duvdevani M, (2011). Xray diffraction and SEM study of kidney stones in Israel: quantitative analysis, crystallite size determination, and statistical characterization. *Environmental Geochemistry and Health*, *33*(*6*), 613–622. doi: 10.1007/s10653-011-9374-6. Epub 2011 Feb 10. PMID: 21308400.

Warty Y, Haryanto F, Fitri LA, Haekal M, Herman H, (2020). Spatial Distribution Analysis on the Deposition Mechanism Complexity of the Organic Material of Kidney Stone. *J Biomed Phys Eng*. *10*(*3*), 273-282. doi: 10.31661/jbpe.v0i0.1104. PMID: 32637371; PMCID: PMC7321398.

CHAPTER III

Theoretical Calculation of Second and Third Virial Coefficients for Kihara Potential

Elif SOMUNCU[1]

Introduction

The determination of thermodynamic properties, transport properties and interaction potentials of atoms and molecules plays an important role in scientific and technological research. To accurately explain the thermodynamic properties of molecules, the nature of intermolecular forces must be fully understood. Therefore, many equations of state have been proposed for the study of such properties of atoms and molecules. To date, many real gas equations of state, which give the gases at high pressure interrelationships between $P-V-T$, have been studied. The most important of these equations of state is the virial equation of state. Virial equation of state has an important feature that determines the interdependent

[1] Assoc. Prof. Dr., Usak University

changes of temperature, pressure, volume, and potential energy of the substance. The equation of state allows the determination of the physical properties of real gases, liquids, liquid mixtures, solids and even the internal structures of stars.

Virial coefficients play a fundamental role in many aspects, including the deviation of the gas from the ideal state to the real state and the determination of intermolecular interactions in various temperature ranges (Kihara et al., 1956; Knoebel and Edmister, 1968; Landau et al., 1980; McQuarrie et al., 1997; Widom, 2002; Boltachev and Baidakov, 2006; Kaplan, 2006; Somuncu and Mamedov, 2022). The study of intermolecular interactions determined according to Virial coefficients allows the investigation of many physical and chemical properties of molecules (Parsafar and Shokouhi, 2006; Abbaspour and Goharshadi, 2010). At the same time, virial coefficients have an important place in the study of thermodynamic properties (internal energy, enthalpy, heat capacity at constant volume, heat capacity at constant pressure, Joule-Thomson coefficient, speed of sound) and transport properties (viscosity, diffusion, thermal conductivity) of gases (Kihara, 1953; Abdulagatov et al, 2002; Ramos-Estrada et al., 2004; Abbaspour and Goharshadi, 2010; Garberoglio et al., 2011; Kim et al., 2013). In addition, virial coefficients are also used in the study of superconductivity production and technological applications, determination of Boyle temperature, thermodynamic properties of industrial gases and hydrocarbons, which are major energy sources (Kihara, 1953; Glasser, 2002; Oh, 2010; Garberoglio et al., 2012; Pai and Bae, 2012). Virial coefficients have an important place in some fields of biology. For example, the second virial coefficient is used to study protein-protein interactions and to determine where the protein crystallises more easily (Deszczynski et al., 2006; Suzette et al., 2008; Gamez et al., 2011; Quigley et al., 2013).

As it is understood, precise calculation of the virial coefficients is required for the analysis of atoms and molecules according to the virial equation. As it is known from the literature, analytical calculation of three, four and higher order virial coefficients remains

one of the important physical problems of today. Due to the difficulty of calculating three, four and higher order virial coefficients, they are usually calculated according to the solid sphere potential, which is easier. Somuncu et al. proposed analytical and numerical methods for the second, third and fourth order virial coefficients using Lennard-Jones (12-6), Sutherland, Kihara, Stockmayer, Morse-Morse-Spline-van der Waals potentials, which are mathematically difficult to work with, in addition to easily calculated potentials such as the solid sphere potential.

Note that, selecting of virial coefficients for atoms and molecules allows precise calculation virial coefficients. Many numerical methods have been developed to calculate virial coefficients using various atomic or intermolecular interaction potentials. It is well known that numerical calculation methods give accurate results for a limited range of parameters and are not suitable for most systems because they are time consuming. Researchers have used a variety of numerical methods to address these shortcomings. However, due to some limitations, these integrals cannot be solved exactly. Numerical methods avoid parameter limits but cannot be applied to a wide range of parameters. Therefore, numerical calculation methods give accurate results for a limited range of parameters. Additionally, numerical methods do not provide exact solutions. Therefore, the computational accuracy and precision of evaluating virial coefficients over different potentials is a very important part of such studies. However, there are almost no analytical methods on this subject. Analytical calculation of higher virial coefficients of gases using interaction potentials between many atoms or molecules is one of today's important physical problems.

The Virial Equation of State

Virial equation, which is a great achievement of statistical mechanics, is directly related to intermolecular interaction potentials (Kihara, 1953; Prausnitz et al., 1999). Virial equation has an important feature that determines the interdependent changes of

temperature, pressure, volume, and potential energy of the substance. Virial equation of state is written following form:

$$\frac{P}{k_B T} = \rho + B_2(T)\rho^2 + B_3(T)\rho^3 + \cdots \quad (1)$$

where $B_2(T)$ is second virial coefficient, $B_3(T)$ is third virial coeffcent, so on (Hirschfelder ve ark., 1954; McQuarrie, 1973; Chiew ve Sabesan, 1999). These coefficients describe the contribution from multiparticle interactions (McQuarrie, 1973; Hutem and Boonchui, 2012; Benjamin et al., 2007). As can be seen from the equation, the N-dimensional problem can be reduced to one, two, three, ... dimensional states in a non-ideal gas (McQuarrie, 1973).

Second Virial Coefficient

The second virial coefficient is very important as it is the first coefficient to depart from the ideal state as the pressure of the gas increases. This coefficient can be analyzed theoretically and experimentally (Graben and Present, 1964). Second virial coefficient is written following as:

$$B_2(T) = -2\pi N_A \int_0^\infty \left(e^{-u(r)/k_B T} - 1\right) r^2 dr \quad (2)$$

where $k_B$is Boltzmann constant, N_A is Avogadro number and $u(r)$is intermolecular interaction energy (Garberoglio et al., 2011). As seen from this equation, the second virial coefficient, which gives the potential energy between two molecules, is physically and chemically related to the intermolecular potential. This coefficient depends on the temperature and the interaction between two molecules for pure substances (McQuarrie, 1973; Prausnitz, 1999; Garberoglio et al., 2011). Today, the second virial coefficient is used for the study of intermolecular potential models from the most complex to the simplest. The second virial coefficient takes negative values at low temperatures and positive values as the temperature

increases (McQuarrine and Simon, 1997). From here, it can be determined in which temperature range the molecule shows repulsive or attractive properties. when it is zero, the gas is in the ideal state. The temperature at which the second virial coefficient is zero is called Boyle temperature (Kihara, 1953; McQuarrine and Simon, 1997). At this temperature, intermolecular repulsive and attractive forces are neglected.

Third Virial Coefficient

The third virial coefficient expresses the departure of the gas from the ideal state due to interactions between three molecules (Kihara, 1953; Prausnitz, 1999). This coefficient can be analyzed experimentally and theoretically (Hirschfelder et al., 1954).

Third virial coefficient is expressed following form:

$$B_3(T) = -\frac{8\pi^2 N_A^2}{3} = \int\int\int f_{12} f_{13}\, f_{23} r_{12} r_{13} r_{23} dr_{12} dr_{13}\, dr_{23} \qquad (3)$$

where f_{ij} is Mayer functions (Hirschfelder et al., 1954). The Mayer function is defined following form:

$$f_{ij} = \left(e^{-u(r)/k_B T} - 1\right) \qquad \text{b} \qquad (4)$$

Here, Mayer function depend on $u\left(r_{ij}\right)$ intermolecular interaction energy (Hirschfelder et al., 1954).

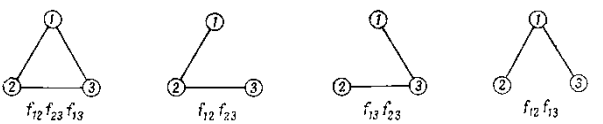

Figure 1. Interaction between three molecules

As can be seen from Figure 1, there are triple interactions as well as double interactions. Therefore, it is more difficult to work with third virial coefficients than second virial coefficients (Graben and Present, 1964).

Fourth Virial Coefficient

The fourth virial coefficient expresses the departure of the gas from the ideal state (Prausnitz, 1999). The fourth virial coefficient

$$B_4(T) = -\frac{3N_A^3}{8V} = \int\int\int 3f_{12}f_{23}f_{34}f_{14} + 6f_{12}f_{23}f_{34}f_{14}f_{13} + f_{12}f_{23}f_{34}f_{14}f_{13}f_{24} \quad (5)$$

where f_{ij} is Mayer functions (Hirschfelder et al., 1954; Boys and Shavitt, 1960).

These coefficients are the sum of the three cluster diagrams shown in Figures 2-4.

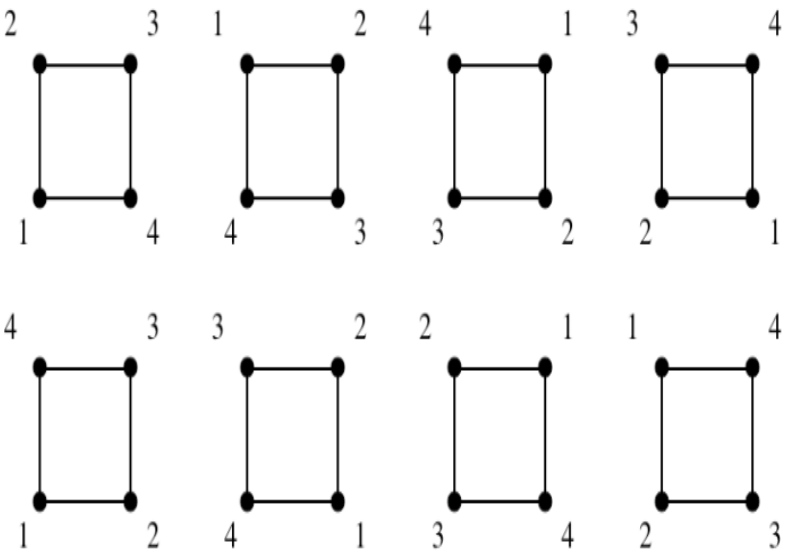

Figure 2. First cluster diagram (1/8)

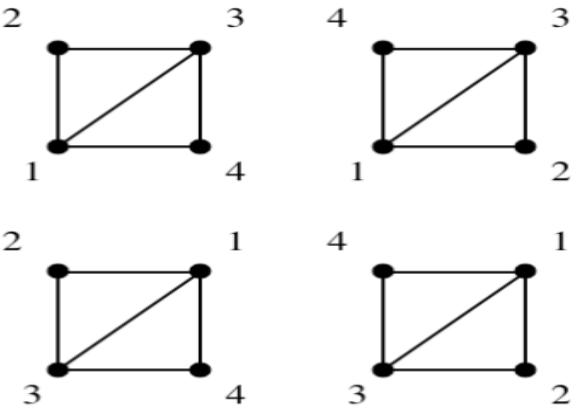

Figure 3. Second cluster diagram (1/4)

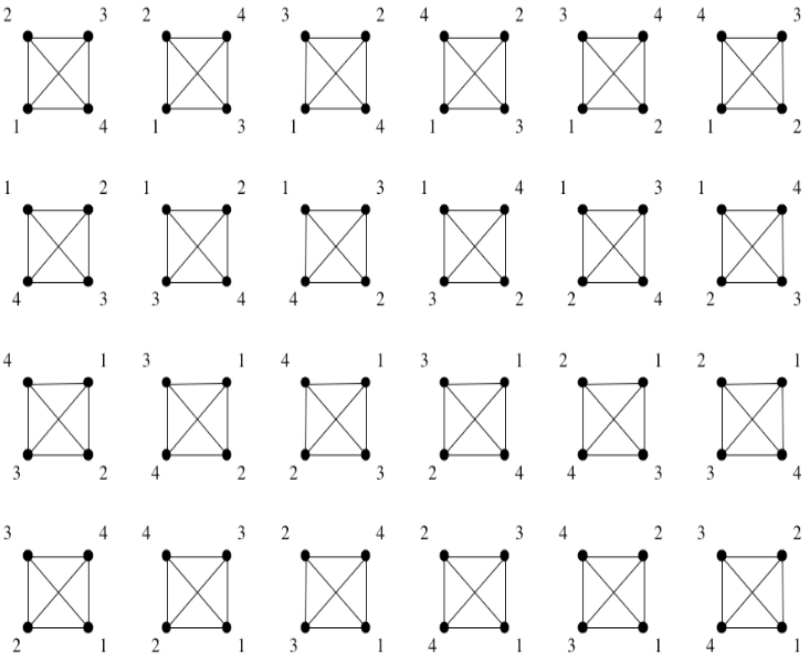

Figure 4. Third cluster diagram (1/24)

Due to the interactions between the four molecules, it is not easy to work with this coefficient experimentally and theoretically. It is very difficult to study the high-order virial coefficients for any suitable potential. These coefficients are calculated for simple potentials such as the solid sphere potential.

As can be seen, virial coefficients are analyzed by determining intermolecular interaction potentials according to the structural properties of the molecule (Kihara, 1953; Hutem and Boonchui, 2012). Therefore, the conformity of the intermolecular interaction potentials used in the calculation of the virial coefficients and their numerical relationship with the selected function are very important. The selected intermolecular interaction potential function should be experimentally and theoretically compatible.

Intermolecular interaction potentials

Intermolecular interaction potentials used in the calculation of the second, third and fourth virial coefficients are determined according to the structural properties of atoms or molecules. Some of the interaction potentials used in analytical and numerical calculations are expressed as follows.

Kihara Potential

The Kihara potential, a three-parameter function, is an equation used to represent the interaction between non-polar molecules. Kihara potential for molecules with spherical nuclei is written following form:

$$u(r) = \begin{cases} \infty & r < d \\ 4\varepsilon\left(\left(\frac{\sigma-d}{r-d}\right)^{12} - \left(\frac{\sigma-d}{r-d}\right)^{6}\right) & r \geq d \end{cases} \quad (6)$$

where d is diameter of the spherical molecule core, ε is energy well depth, σ is the radius of collision (Prausnitz et al., 1999).

Definition of Second Virial Coefficient with Kihara Potential

The new analytical formula has been derivate to calculate precision and correctly second virial coefficient over Kihara potential. The substituting Eq. (5) into Eq. (2), we obtained following formula:

$$B_2(T) = -2\pi N_A \left(\int_0^d (e^{-\infty} - 1) r^2 dr + \int_d^\infty \left(e^{-\frac{4\varepsilon}{k_B T}\left(\left(\frac{\sigma-d}{r-d}\right)^{12} - \left(\frac{\sigma-d}{r-d}\right)^{6}\right)} - 1 \right) r^2 dr \right) \quad (7)$$

By taking partial integration of Eq. (7) and using the series expression in Eq. (7), we have obtained following analytical formula (Somuncu et al., 2020):

$$H[u,k] = \lim_{N\to\infty} \sum_{t=0}^{N} \frac{(4\varepsilon/k_B T)^t}{t!} (\sigma - d)^{6+6t} u^{\left(-\frac{6t+k}{12}\right)} \quad (8)$$

$$B_2(T) = \frac{2\pi N_A d^3}{3} + \frac{8\pi N_A \varepsilon}{3k_B T}\left((\sigma-d)^6 \left(d^3 H\left[\frac{4\varepsilon/k_B T}{(\sigma-d)^{-12}}, 12\right] + 3d^2 H\left[\frac{4\varepsilon/k_B T}{(\sigma-d)^{-12}}, 11\right] + H\left[\frac{4\varepsilon/k_B T}{(\sigma-d)^{-12}}, 9\right]\right) - \right.$$
$$\left. + \frac{1}{2}\left(d^3 H\left[\frac{4\varepsilon/k_B T}{(\sigma-d)^{-12}}, 6\right] + 3d^2 H\left[\frac{4\varepsilon/k_B T}{(\sigma-d)^{-12}}, 5\right] + 3dH\left[\frac{4\varepsilon/k_B T}{(\sigma-d)^{-12}}, 4\right] + H\left[\frac{4\varepsilon/k_B T}{(\sigma-d)^{-12}}, 3\right]\right)\right) \quad (15) \quad (9)$$

The Eq.(9) has been applied to molecule $n-C_5H_{12}$. The parameters of the Kihara potential for $n-C_5H_{12}$ is d=1.13139, $\varepsilon/k_B = 837.82$ and $\sigma = 5.029$ (Prausnitz et al., 1999). The calculation results have given in Table 1.

Tablo 1. Compared with other studies of second virial coefficient for $n-C_5H_{12}$

$T(K)$	This work	Mathematica numeric results	Experimental (Dymond et al., 2018)
259.55	-1742.37	-1786.21	-1610
300.00	-1161.74	-1205.58	-1159
351.20	-772.616	-816.454	-783
401.00	-556.693	-600.531	-578
453.15	-413.21	-457.048	-445
523.15	-289.428	-333.266	299
548.16	-256.826	-300.664	-265
623.15	-181.729	-225.567	-192
648.15	-162.216	-206.055	-174

As seen from Table 1, the accurate and precision of results of second virial coefficient for $n-C_5H_{12}$ are in good agreement with experimental data (Dymond et al., 2018).

Definition of Third Virial Coefficient with Kihara Potential

Three atomic system for the determination of the third virial coefficient:

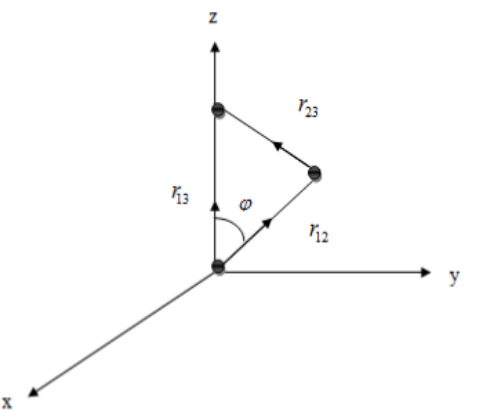

Figure 5. Three atom system

The values of r_{12}, r_{13} and r_{23} have been defined following form:

$$|r_{13}-r_{12}|=r_{23}=\sqrt{r_{12}^2+r_{13}^2-2r_{12}r_{13}\cos\varphi}$$

$$dr_{13}=4\pi r_{13}^2 dr_{13}$$

$$dr_{12}=2\pi r_{12}^2 dr_{12}\sin\varphi d\varphi$$

$$\eta=\cos\varphi$$

The considering for r_{12}, r_{13}, r_{23} and η values, the integrate formula for accurate and precise calculation of the third viral coefficient with Kihara potential has been presented following form:

$$B_3(T^*)=\frac{6}{(1+a^*)^6}\left[\int_0^\infty r_{12}^{*2}\left(e^{-\frac{4}{T^*}\left(\left(r_{12}^*-a^*\right)^{-12}-\left(r_{12}^*-a^*\right)^{-6}\right)}-1\right)\int_0^\infty r_{13}^{*2}\left(e^{-\frac{4}{T^*}\left(\left(r_{13}^*-a^*\right)^{-12}-\left(r_{13}^*-a^*\right)^{-6}\right)}-1\right)\right.$$
$$\left.\int_{-1}^{1}\left(e^{-\frac{4}{T^*}\left(\left(\sqrt{r_{12}^2+r_{13}^2-2r_{12}r_{13}\eta}-a^*\right)^{-12}-\left(\sqrt{r_{12}^2+r_{13}^2-2r_{12}r_{13}\eta}-a^*\right)^{-6}\right)}-1\right)dr_{12}^*dr_{13}^*d\eta\right] \quad (10)$$

where $r_{ij}^*=r_{ij}/\sigma$ ve $d^*=d/\sigma-d$ 'dir. The numerical formula for third virial coefficient with Kihara potential has been obtained following form:

$$B_3(T)=\frac{12}{(1+d^*)^6}\left[\int_0^\infty\left(e^{-\frac{4}{T^*}\left(\left(r_{12}^{*2}-d^*\right)^{-12}-\left(r_{12}^{*2}-d^*\right)^{-6}\right)}\right.\right.$$
$$\left.\left.-1\right)r_{12}^{*2}\int_0^\infty\left(e^{-\frac{4}{T^*}\left(\left(r_{13}^{*2}-d^*\right)^{-12}-\left(r_{13}^{*2}-d^*\right)^{-6}\right)}-1\right)r_{13}^{*2}ddr_{12}^*dr_{13}^*\right]$$

$$-\frac{6}{(1+d^*)^6}\left[\int_0^\infty \left(e^{-\frac{4}{T^*}\left((r_{12}^{*2}-d^*)^{-12}-(r_{12}^{*2}-d^*)^{-6}\right)}-1\right) r_{12}^{*2}\int_0^\infty (-1)\, r_{13}^{*2}\, dd r_{12}^* dr_{13}^*\right]\right]$$

$$\int_{-1}^{1} e^{-\frac{4}{T^*}\left(\left(\sqrt{r_{12}^2-2r_{12}r_{13}\eta}-d^*\right)^{-12}-\left(\sqrt{r_{12}^2-2r_{12}r_{13}\eta}-d^*\right)^{-6}\right)}\Bigg] dr_{12}^* dr_{13}^* d\eta \qquad (11)$$

Semi-analytical formula for accurate and precise calculation of the third viral coefficient with Kihara potential has been presented following form (Somuncu and Mamedov, 2018):

$$B_3(T^*) = \frac{12}{(1+d^*)^6} I(T^*) - \frac{6}{(1+d^*)^6} K(T^*) \qquad (12)$$

$I(T^*)$ and $K(T^*)$ in Eq. (12) have derivated following as:

$$I\left(T^*\right)=\left[\int_0^\infty r_{12}^{*2}\left(e^{-\frac{4}{T^*}\left(\left(r_{12}^*-a^*\right)^{-12}-\left(r_{12}^*-a^*\right)^{-6}\right)}-1\right)\int_0^\infty r_{13}^{*2}\left(e^{-\frac{4}{T^*}\left(\left(r_{13}^*-a^*\right)^{-12}-\left(r_{13}^*-a^*\right)^{-6}\right)}-1\right)dr_{12}^* dr_{13}^*\right] \qquad (13)$$

$$\begin{aligned} I\left(T^*\right)=\Bigg[& -\frac{a^{*3}}{3}+\frac{1}{6}\sum_{n=0}^{N}\frac{1}{n!}\Bigg(-2\left(\frac{4}{T^*}\right)^{\frac{n}{2}+\frac{1}{4}}\Gamma\left(\frac{n}{2}+\frac{3}{4}\right)-6a^*\left(\frac{4}{T^*}\right)^{\frac{n}{2}+\frac{1}{6}}\Gamma\left(\frac{n}{2}+\frac{5}{6}\right)- \\ & 6a^{*2}\left(\frac{4}{T^*}\right)^{\frac{n}{2}+\frac{1}{12}}\Gamma\left(\frac{n}{2}+\frac{11}{12}\right)+\left(\frac{4}{T^*}\right)^{\frac{n}{2}+\frac{3}{4}}\Gamma\left(\frac{n}{2}+\frac{1}{4}\right)+ \\ & 3a\left(\frac{4}{T^*}\right)^{\frac{n}{2}+\frac{2}{4}}\Gamma\left(\frac{n}{2}+\frac{1}{3}\right)+3a^{*2}\left(\frac{4}{T^*}\right)^{\frac{n}{2}+\frac{7}{13}}\Gamma\left(\frac{n}{2}+\frac{5}{12}\right)\Bigg)\Bigg]^2 \end{aligned} \qquad (14)$$

$$K\left(T^*\right)=\left[\int_0^{\infty} r_{13}^{*2}\left(e^{-\frac{4}{T^*}\left(\left(r_{12}^*-a^*\right)^{-12}-\left(r_{12}^*-a^*\right)^{-6}\right)}-1\right)\int_0^{\infty} r_{13}^{*2}\left(e^{-\frac{4}{T^*}\left(\left(r_{13}^*-a^*\right)^{-12}-\left(r_{13}^*-a^*\right)^{-6}\right)}-1\right)\right.$$
$$\left.\int_{-1}^{1}\left(e^{-\frac{4}{T^*}\left(\left(\sqrt{r_{12}^2+r_{13}^2-2r_{12}r_{13}\eta}-a^*\right)^{-12}-\left(\sqrt{r_{12}^2+r_{13}^2-2r_{12}r_{13}\eta}-a^*\right)^{-6}\right)}\right)dr_{12}^*dr_{13}^*d\eta\right] \quad (15)$$

Tablo 2. Reduced second virial coefficient for different d values

$T(K)$ \ d	This work 0.00	Lennard-Jones (12-6) potential 0.00	0.05	0.1	0.5	0.75
0.50	-40.1638	-40.1638	-31.9503	-25.5726	-4.78344	-1.54602
0.80	-0.84915	-0.84915	-0.394662	-0.072073	0.593839	0.538579
1.00	0.429769	0.429769	0.518713	0.569523	0.508616	0.411836
2.00	0.437073	0.437073	0.417365	0.399518	0.321698	0.31028
3.00	0.352309	0.352309	0.345039	0.339313	0.329788	0.340075
4.00	0.3266	0.3266	0.325697	0.32567	0.343447	0.360938
5.00	0.315082	0.315082	0.3176	0.32058	0.35205	0.372907
6.00	0.307625	0.307625	0.312248	0.317037	0.35664	0.379477
10.00	0.286068	0.286068	0.294367	0.302369	0.356765	0.383438

In Table 2, the accurate of the obtained reduced third virial coefficient is shown through its comparison with different results obtained using Lennard-Jones potential results (Hirschfelder et al., 1954). Also, the Kihara potential gives the L-J (12-6) potential when the d potential parameter is equal to zero (Hirschfelder et al., 1954). Therefore, the calculated results for the reduced third virial coefficient have been compared with the obtained results from d=0 and have demonstrated that the results are in good agreement in Table 2.

References

Abbaspour, M.& Goharshadi, E. K. (2010) Computation of some thermodynamics,transport, structural properties, and new equation of state for fluid neon using a new intermolecular potential from molecular dynamics simulation *Theoretical Chemistry Accounts*, *127* (5/6), 573-585. Doi: 10.1007/s00214-010-0751-5.

Abdulagatov, A. I., Kaplun, A. B., Meshalkin, A. B., Abdulagatov, I. M. & Stepanov, G.V. (2002) Second caloric virial coefficients for real gases and combined spherical symmetric potential for simple molecular interactions *The Journal of Chemical Thermodynamics*, *34* (12), 2049–2072.Doi: 10.1016/S0021-9614(02)00259-8.

Benjamin, K. M., Singh, J. K., Schultz, A. J. & Kofke, D. A. (2007) Higher-order virial coefficients of water models *Journal of Physical Chemistry B 111* (39), 11463-11473.Doi: 10.1021/jp0710685.

Boltachev, G. S. & Baidakov, V. G. (2006) The Second Virial Coefficients of Simple Fluids. *High Temperature*, *44* (1), 83-90. Doi: 10.1007/s10740-006-0009-z.

Boys S. F. & Shavitt, I. (1960) Intermolecular forces and properties of fluids. The automatic calculation of higher virial coefficients and some values of fourth coefficient for the Lennard-jones potential *Proceedings of the Royal Soceity A 254*, 487-498. Doi: 10.1098/rspa.1960.0034.

Chiew, Y. C. & Sabesan, V. (1999) Second virial coefficients of Lennard–jones chains *Fluid Phase Equilibria*, *155* (5), 75-83. Doi: 10.1016/S0378-3812(98)00457-9.

Deszczynski, M., Harding, S. E. & Winzor, D. J. (2006) Negative second virial coefficients as predictors of protein crystal growth: evidence from sedimentation equilibrium studies that refutes the designation of those light scattering parameters as

osmotic virial coefficients *Biophysical Chemistry*, *120* (2), 106 – 113. Doi: 10.1016/j.bpc.2005.10.003.

Dymond, J. H., Marsh, K. N., Wilhoit, R. C. & Wong, K. C. (2018). *Virial Coefficient of pure Gases and Mixtures*. New York: Springer-Verlag Berlin Heidelberg.

Gamez, F., Lago, S., Plaza-Reyes, A. & Gonzalez-Claderon, A. (2011) Second virial coefficients of mesoogenic international potentials *Journal Molecular Liquids*, *164* (1-2) 153-156. Doi: 10.1016/j.molliq.2011.07.009.

Garberoglio, G., Moldever, M. R. & Harvey, A. H. (2011) Improved first-principles calculation of the third virial coefficient of Helium *Journal of Research of the National Institute of Standards and Technology*, *116* (4), 729-742. Doi: 10.6028/jres.116.016.

Garberoglio, G., Jankowski, P., Szalewicz, K. & Harvey, A. H. (2012) Second virial coefficents of H_2 and its isotopologues from a six-dimensional potential *Journal of Chemical Physics*, *137* (15), 154308- 154319. Doi: 10.1063/1.4757565.

Glasser, M. L. (2002) Second virial coefficient for a Lennard-Jones (2*n*−*n*) system in d dimensions and confined to a nanotube surface *Physics Letters A, 300* (4-5), 381 384. Doi: 10.1016/S0375-9601(02)00814-9.

Graben, H. W. & Present, R. D. (1964) Third virial coefficient for the Sutherland (∞, ν) potential *Rev. Mod. Phys.*, 1025-1033. Doi: 10.1103/RevModPhys.36.1025.

Hutem, A. & Boonchui, S. (2012) Numerical evaluation of second and third virial coefficients of some inert gases via classical cluster expansion *J. Math. Chem.*, *50* (5), 1262-1276. Doi: 10.1007/s10910-011-9966-5.

Kaplan, I. G. (2006). *Intermolecular Interactions: Physical Picture. Computational Methods and Model Potentials*. New York: John Wiley & Sons.

Kihara, T. (1953) Virial coefficients and models of molecules in gases *Review of Modern Physics, 25* (4), 831-843. Doi: 10.1103/RevModPhys.25.831.

Kihara, T., Midzünö, Y. & Kaneko, S. (1956). Virial coefficients and intermolecular potential for small nonspherical molecules *Journal of the Physical Soceity of Japan, 11* (4), 362-366. Doi:10.1143/JPSJ.11362.

Kim, H. M., Schultz, A. J. & Kofke, D. A. (2013) Second through fifth virial coefficients for models' methane-ethane mixtures *Fluid Phase Equilibria, 351* 69-73. Doi: 10.1016/j.fluid.2012.10.014.

Knoebel, D. H. & Edmister, W. C. (1968) Second virial coefficients of binary mixtures of Benzene with Methanol, Ethanol, Acetone, and Diethyl Ether *Journal of Chemical Engineering Data, 13* (3), 312–317. Doi: 10.1021/je60038a005.

Landau, L. D. & Lifshitz, E. M. (1980) *VII. Non-Ideal Gases. Statistical Physics*. Pergamon.

McQuarine, D. A. (1973) *Statistical Mechanics.* New York: Harper & Row.

McQuarrine, D. A. & Simon, J. D. (1997) *Physical Chemistry: A Molecular Approach*. University Science Book.

Oh, S. K. (2010) Extending the group contribution concept using Kihara potential to Perfluorinated n-alkanes $C_nF_{2n+2}\left(n=1-6\right)$ for estimating thermophysical *Fluid Phase Equilibria, 288* 87-95. Doi: 10.1016/j.fluid.2009.10.023.

Ramos-Estrada, M., Tellez-Morales, R., Iglesias-Silva, G. A. & Hall, K. R. (2004) A generalized correlation for the second virial coefficient based upon the Stockmayer potential *Latin American Applied Research, 34* (1), 34-41.

Pai, S. J. & Bae, Y. C. (2012) Understanding physical properties of hydrocarbon polymers using an equation of

state developed from semi soft-core potential function *Fluid Phase Equilibria, 317* 15-24. Doi: 10.1016/j.fluid.2011.12.020.

Parsafar, G. A. & Shokouhi, M. (2006) Modification of a new potential model used for calculation of the second virial coefficient and zero density transport properties *Molecular Physics, 104* (20-21), 3269-3280. Doi: 10.1080/00268970601082887.

Prausnitz, J. M., Lichtenthaler, R. N. & Azevedo, E. G. de (1999) *Fugacities in Gas Mixtures. Molecular Thermodynamics of Fluid-Phase Equilibria.* New Jersey: Prentice-Hall.

Suzette, L.L., Pabit, A., Lamb, J. S., Park, H. Y. & Pollack, L. (2008) Closing the lid on DNA end-to-end stacking interactions *Applied Physics Letters, 92* (22), 223901-223903. Doi: 10.1063/1.2937402.

Somuncu, E, Mamedov, B. A. & Askerov, I. M. (2018) Theoretical study of third virial coefficient with Kihara potential *Canadian Journal of Physics* Doi: 10.1139/cjp-2017-0705.

Somuncu, E., Emek, M. & Mamedov, B. A. (2020) Unified analytical formulae of second virial coefficient with Kihara potential and its application to real gases Acta Physica Polonica A, 137 (3) 293-299. Doi: 10.12693/APhysPolA.137.293.

Somuncu, E. & Mamedov, B. A. (2022) Evaluation of specific heat capacity and speed of sound of fluids by using the quantum correction to second virial coefficient with Kihara potential. *The European Physical Journal Plus,137 298* Doi: 10.1140/epjp/s13360-022-02503-2.

Quigley, A., Heng, J. Y. Y., Liddell, J. M. &Williams, D. R. (2013) The accurate measurement of second virial coefficients using self-interaction chromatography: experimental consideration *European Journal of Pharmaceutics and Biopharmaceutics*, *85* (3), 1103-1111. Doi: 10.1016/j.ejpb.2013.04.004.

Widom, B. (2002) *The Non-Ideal Gas. Statistical Mechanics: A Concise Introduction for Chemists*. New York: Cambridge Universty Press.

In Molecular Analysis: The Mystery of the Realm of Spectroscopic Techniques and Thermodynamic Properties

Dear Readers,

We are excited to bring you this work that will take you deep into the molecular world. Science is a reflection of humanity's passion for exploring unknown frontiers. This passion is constantly fueled by the desire to acquire new knowledge and insights. This book brings together a series of important studies that aim to delve deeper into scientific knowledge. "In Molecular Analysis: The Mystery of the Realm of Spectroscopic Techniques and Thermodynamic Properties" aims to provide readers who wish to understand the subtle fabric of science with a guide to unlock the doors of the molecular world and unravel its mysteries.

The overall goal of our book is to explore molecular analysis through unique perspectives arising from the combination of spectroscopic techniques and thermodynamic properties. The combination of thermodynamic principles with the insights provided by spectroscopic techniques is the main focus of this book in order to understand and extend the understanding of the complexity of the molecular world.

This book aims to not only provide readers with a scientific perspective, but also to inspire them to push the boundaries of the molecular world by arousing their scientific curiosity. It is intended as a comprehensive resource for both students and experts to understand the fundamentals of molecular analysis and deepen their knowledge in this field. We hope that "In Molecular Analysis: The Mystery of the Realm of Spectroscopic Techniques and Thermodynamic Properties" will take you on this magical journey, bring you together with science and deepen your curiosity.

We wish you a good reading.

BİDGE